TOPOLOGICAL OPTICS

Fractal photonic topological insulators

Tobias Biesenthal[1], Lukas J. Maczewsky[1], Zhaoju Yang[2]*, Mark Kremer[1], Mordechai Segev[3], Alexander Szameit[1]*, Matthias Heinrich[1]*

Topological insulators constitute a newly characterized state of matter that contains scatter-free edge states surrounding an insulating bulk. Conventional wisdom regards the insulating bulk as essential, because the invariants that describe the topological properties of the system are defined therein. Here, we study fractal topological insulators based on exact fractals composed exclusively of edge sites. We present experimental proof that, despite the lack of bulk bands, photonic lattices of helical waveguides support topologically protected chiral edge states. We show that light transport in our topological fractal system features increased velocities compared with the corresponding honeycomb lattice. By going beyond the confines of the bulk-boundary correspondence, our findings pave the way toward an expanded perception of topological insulators and open a new chapter of topological fractals.

Topological insulators (TIs) (*1*) have permeated various fields of physics, such as photonics (*2*–*5*), cold atoms (*6*), mechanics (*7*), acoustics (*8*), electronics (*9*), and exciton-polaritons (*10*). Fractals, on the other hand, are a class of systems in which topological phenomena still remain elusive. By definition, fractals are objects in which each constituent exhibits the same character as the whole (*11*) (see also supplementary text). Photonics, in particular, allows fractals to unfold their multifaceted influence, for example, as fractal diffraction (*12*), complex lasing modes (*13*), temporal fractals forming from self-similar spatial structures (*14*), anomalous transport governed by the fractal dimension (*15*), or flatbands in fractal-like photonic lattices (*16*).

The Sierpinski gasket (*17*) is one of the best-known examples of an exact fractal and has been theoretically predicted to allow for topological edge states when exposed to an appropriate modulation (*18*). The structure emerges when an equilateral triangle is iteratively partitioned into four identical segments while leaving the central one as void. In this procedure, each subsequent step constitutes a "generation." Appearing self-similar under arbitrary degrees of magnification, the lattice exhibits symmetry across scales. In contrast to quasi-crystals, whose bulk exclusively displays long-range order but not self-similarity (*19*, *20*), each segment of the Sierpinski gasket replicates not only the statistical properties but also the very structure of the whole (*17*). Being a nowhere-dense, locally connected metric continuum, it features a noninteger Hausdorff dimension of $d = \log_2 3 \approx 1.585$ with vanishing Lebesgue measure over its area (*11*). Notably, the Sierpinski gasket does not contain any bulk in the conventional sense and therefore falls outside the purview of a cornerstone of topological physics: the bulk-edge correspondence (*21*). Despite defying characterization by conventional (bulk) topological invariants such as the Chern (*22*) or winding number (*23*), it has been suggested that the Sierpinski gasket may serve as the underlying structure for fractal TIs (*18*, *24*, *25*). Yet, the Sierpinski gasket is composed of about one-third fewer sites than the underlying honeycomb lattice, and a random removal of such a large proportion of bulk sites generally destroys the nontrivial characteristics of honeycomb-based TIs (*18*). Moreover, recent observations in self-assembled thin films seemed to indicate that fractal structuring suppresses the intrinsic topological properties of the host system (*26*).

Here, we report the observation of fractal TIs and demonstrate that periodically driven photonic lattices with Sierpinski geometry support topologically protected chiral edge states, despite the absence of any actual bulk. Our work hints at the possibilities of observing topological transport in other fractal platforms with two or more spatial dimensions, such as the Cantor dust, the Cantor cube, and the Sierpinski tetrahedron.

We constructed our fractal TI from helically driven photonic lattices of coupled waveguides (*2*). Without modulation, the structure remains topologically trivial and lacks protected transport or any property of a topological nature. The transport dynamics in our structure can be described by a set of tight-binding coupled-mode equations (*27*)

$$i\frac{\partial}{\partial z}\psi_n = \sum_{\langle m \rangle} c e^{i\vec{A}(z)\cdot\vec{r}_{m,n}}\psi_m$$

where z is the optical axis, ψ_n is the electric field amplitude in the nth waveguide, c is the intersite-hopping strength, and $\vec{r}_{m,n}$ is the displacement vector pointing from waveguide m to waveguide n and summation over nearest neighbors $\langle m \rangle$. The periodic driving of the lattice induces a gauge vector potential $\vec{A}(z) = kR\Omega(\sin\Omega z, -\cos\Omega z, 0)$, where k is the wavenumber of the light in the medium, R is the radius, and Ω is the longitudinal frequency of the helix corresponding to a periodicity of $T = 2\pi/\Omega$.

To compute the eigenvalue spectrum, we diagonalized the unitary evolution operator for one period (*27*). Figure 1A shows a fourth-generation Sierpinski gasket of static waveguides [i.e., $\vec{A}(z) = 0$]. Comparing its numerically calculated fractal eigenvalue spectrum (Fig. 1B) with that of a static honeycomb lattice (Fig. 1C) of the same dimensions, the notable differences to the continuous eigenvalue spectrum (Fig. 1D) of the latter become apparent: Whereas the honeycomb exhibits a single gap (with, owing to its finite size, a number of trivial states in its center), the eigenvalue spectrum of the fractal hosts multiple gaps that increase in complexity for higher generations. Both the Sierpinski gasket and the honeycomb lattice are topologically trivial and feature degenerate zero-energy mid-gap states. In turn, modulating the trajectories of the waveguides in a helical fashion [$\vec{A}(z) \neq 0$] (Fig. 1E) transforms these mid-gap states into topological edge states (Fig. 1F). To illustrate their topological character, we compute the real-space Chern number $\mathcal{C}^{(\mathrm{rs})}$ (*18*), represented as color-coded vertical stripes in Fig. 1, B, D, F, and H. We note that whereas $\mathcal{C}^{(\mathrm{rs})}$ is globally zero in the static systems (Fig. 1, B and D), the driven Sierpinski lattice exhibits nontrivial behavior [$\mathcal{C}^{(\mathrm{rs})} \neq 0$] in multiple regions. As shown in Fig. 1F, the central region of the spectrum is dominated by topological states [$\mathcal{C}^{(\mathrm{rs})} = +1$] circulating along the outer boundary in a counterclockwise direction and in opposite fashion around inner edges—a direct manifestation of the topological fractal nature of the Floquet Sierpinski gasket. In higher generations of the fractal, more and more voids and associated inner edges emerge. By inductive reasoning, it follows that every internal edge of fourth- or higher-generation gaskets supports at least one protected edge state. By contrast, the conventional honeycomb TI (Fig. 1G) only exhibits unidirectional edge states with $\mathcal{C}^{(\mathrm{rs})} = +1$ along its outer perimeter, embedded between two bulk bands with $\mathcal{C}^{(\mathrm{rs})} = 0$ (Fig. 1H).

For our experiments, we used laser-direct-written photonic waveguide lattices (see methods

[1]Institut für Physik, Universität Rostock, Albert-Einstein-Straße 23, 18059 Rostock, Germany. [2]Interdisciplinary Center for Quantum Information, Zhejiang Province Key Laboratory of Quantum Technology and Device, Department of Physics, Zhejiang University, Hangzhou 310027, Zhejiang Province, China. [3]Physics Department, Electrical Engineering Department, and Solid State Institute,Technion–Israel Institute of Technology, Haifa 32000, Israel.
*Corresponding author. Email: zhaojuyang@zju.edu.cn (Z.Y.); alexander.szameit@uni-rostock.de (A.S.); matthias.heinrich@uni-rostock.de (M.H.)

for details). To ensure that our system conforms to the requirements of an exact fractal, we made sure that the individual constituent waveguides are all identical and therefore would be suitable building blocks for arbitrary generations of our fractal system. First, we studied bulk transport in the fractal Sierpinski lattice (Fig. 2A) using the honeycomb lattice (Fig. 2B) as a reference. To this end, we recorded the discrete diffraction patterns obtained by launching light into each of the nine sites (marked "1" to "9" in the respective inserts) comprising the smallest plaquette of the fourth-generation Sierpinski gasket. The ensemble of diffraction patterns obtained from the equivalent single-site excitations in the honeycomb lattice served as reference. To allow for a direct quantitative comparison of the respective spread, we calculated the inverse participation ratios (IPRs) of the recorded intensity patterns for sites 1 to 9 and normalized them according to their respective ensemble average in each system. Under static conditions (Fig. 2C), the specific choice of the injection site in the Sierpinski structure has a profound impact on whether light diffracts widely (Fig. 2D) or remains tightly localized (Fig. 2E). In agreement with theoretical findings (*28*), this behavior directly results from the fractal nature of the Sierpinski gasket and is reflected in the wide standard deviation of the normalized IPR ($\sigma_{IPR}^{S,static} \approx 0.40$). By contrast, in the honeycomb lattice, despite generally spreading further (Fig. 2, F and G), the resulting normalized IPR is much more uniform ($\sigma_{IPR}^{H,static} \approx 0.18$). In the Floquet regime (Fig. 2H), the average spread in the driven Sierpinski lattice actually increases by more than 20% compared with that of the static fractal lattice. At the same time, the decreasing standard deviation ($\sigma_{IPR}^{S,driven} \approx 0.22$) shows the impact on the transport properties in the fractal TI (Fig. 2, I and J). As in all Floquet TIs, the edge states have nonzero group velocity—a feature that can be used in various applications, for example, to force injection locking of many laser emitters (*29*). Because the Sierpinski gasket lacks bulk states and simultaneously supports a larger number of topological edge states than a driven honeycomb of equivalent size, its single-site excitations are generally more likely to project onto at least one such state of nonzero velocity. By contrast, bulk diffraction in the driven honeycomb (Fig. 2, K and L) becomes more homogeneous ($\sigma_{IPR}^{H,driven} \approx 0.06$), whereas transport decreases by more than 30% in the ensemble average.

Next, we observed the topologically protected unidirectional states along the outer perimeter (Fig. 3, A to J, and fig. S4) and explored a hybrid structure: partially fractal and partially honeycomb. Driven by the same modulation, it has been predicted that the perimeter states seamlessly combine (*18*). As shown in Fig. 3, K to O, we directly injected a broad beam of appropriate phase front tilt at the edge of a rhomboid array composed of a Sierpinski gasket and a honeycomb triangle of the same size. This direct excitation (Fig. 3K) injects a substantial fraction of light into the topological Sierpinski perimeter state, which then freely continues along the honeycomb edge (Fig. 3L) after circumnavigating the corner that marks the domain boundary (Fig. 3M). Conversely, when the topological edge state is excited in the honeycomb lattice (Fig. 3N), it readily transitions into the fractal lattice and continues along its perimeter (Fig. 3O).

Having confirmed the compatibility of Sierpinski and honeycomb edge transport, we compared the properties of the topological edge states in the two systems in greater detail. To facilitate quasi-energy–specific excitations of states, we appended planar waveguide arrays to a corner (Fig. 4A). These "straws" of driven waveguides enable synthesizing input wave packets that populate edge states with high specificity and, owing to the equivalent corner geometry of the Sierpinski and honeycomb triangles, provides identical local coupling conditions required for quantitative comparisons (see methods). The measured edge-state occupation ratio for the Sierpinski gasket is shown in Fig. 4B. We find that straw wave numbers that correspond to quasi-energies outside the topological gap result in notable

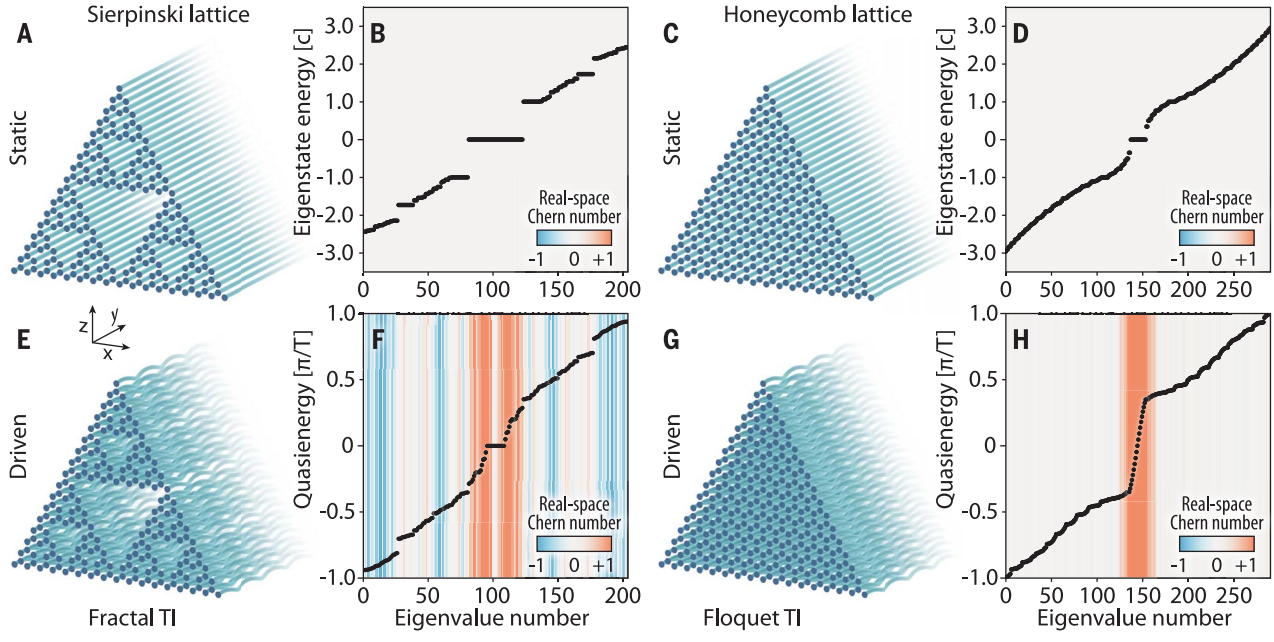

Fig. 1. Fractal TIs. (**A** to **H**) Comparison of a fourth-generation Sierpinski gasket (A) and its numerically calculated eigenvalue spectrum (B) with a photonic honeycomb lattice (C) of the same edge length and its respective eigenvalue spectrum (D). Both static systems are topologically trivial and exhibit a number of degenerate mid-gap states. Uniform periodic modulation via helical trajectories transforms the Sierpinski gasket into a Floquet fractal TI (E) and creates topological edge states from the mid-gap flatband (F). Spatially, they reside on the outer perimeter and the inner edges. Under identical modulation (G), the mid-gap states of the honeycomb lattice likewise transform into topological edge states (H). The real-space Chern number (+1 for topologically protected states) is illustrated by color-coded vertical stripes in (B), (D), (F), and (H). The topological nature of the driven Sierpinski lattice is also confirmed by the Bott index (see fig. S1); representative mode profiles are provided in fig. S2.

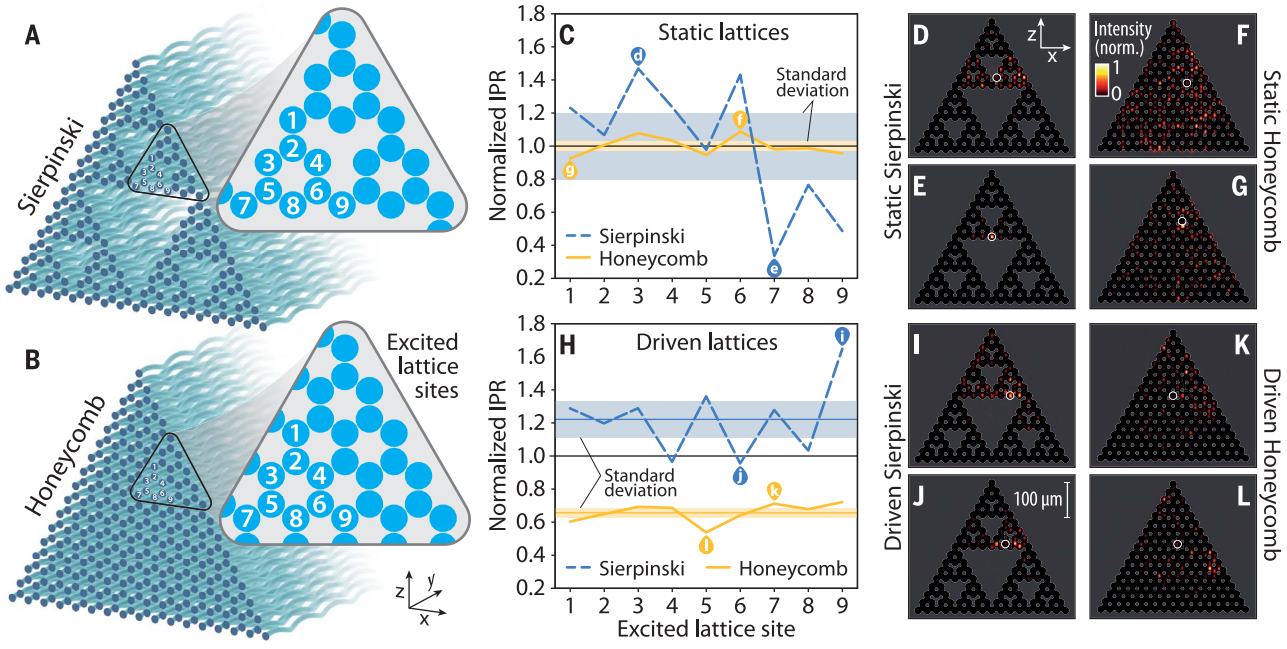

Fig. 2. Bulk transport in fractal and honeycomb lattices. (**A** and **B**) Transport properties of the Sierpinski gasket (A) and the honeycomb lattice (B) as quantified by the normalized IPR of diffraction patterns from representative sites (marked one to nine in the respective inserts). (**C** to **G**) Static regime: In the Sierpinski gasket (C), the specific choice of the injection site determines whether light diffracts strongly (D) or remains tightly localized (E). By contrast, light spreads widely across the honeycomb lattice regardless of the specific injection site [(F) and (G)]. (**H** to **L**) Topological regime: Single-site excitations in the driven Sierpinski lattice (H) exhibit substantially larger broadening [(I) and (J)] compared with the static case, whereas the overall range of variation is decreased. By contrast, bulk transport in the honeycomb is substantially decreased [(K) and (L)]. As a guide to the eye, the standard deviations around the average normalized IPR values are shown as shaded regions in (C) and (H). The observed diffraction patterns corresponding to the largest and smallest broadening are shown in (D) to (G) and (I) to (L), respectively. Moreover, the outlines of the respective lattices are indicated by a semitransparent overlay. The full sets of observed diffraction patterns are shown in fig. S3.

penetration into the lattice interior (Fig. 4C). On the other hand, pronounced population of the topological edge state occurs at the resonant angle of excitation (Fig. 4D). Similar to the behavior in the honeycomb (Fig. 4, E to H), these observations provide direct evidence for the existence of a topological band gap and associated chiral states at the perimeter of the fractal Sierpinski structure. Beyond demonstrating the existence of topological states, evaluating the angle-dependent occupation ratio of the outer perimeter provides a quantitative estimate of the width of the corresponding topological gap. Along these lines, our measurements show that these widths in the Sierpinski gasket (Δ^{S} = 1.95 cm^{-1}) are similar to those of the honeycomb (Δ^{H} = 1.95 cm^{-1}) lattice, determined as full width at half maximum of Gaussian fits of the respective resonances in the quasi-energy (see Fig. 4, B to F, and fig. S7).

Notably, we find that the fractal perimeter states systematically outpace their counterparts in the conventional lattice. As depicted in Fig. 4, I and J, the center of mass n_{E} of their Gaussian envelope is found several lattice sites further along the perimeter than for comparable excitation placements n_{x} in the straw, corresponding to an ~11% larger velocity in the fractal (Fig. 4K and figs. S8 and S9). This higher rate of topological transport is particularly surprising because the Sierpinski gasket has many more corners than the honeycomb, which normally act as defects (*2*) and tend to stall transport as the edge state navigates around them. We attribute the observed speed increase to the absence of bulk sites that gives propagating edge wave packets less opportunities to linger. Numerical investigations of the dispersive properties of these dynamics indicate that the self-similar hierarchy of voids in the fractal lattice serves to selectively annihilate topological states that, in the conventional honeycomb system, would propagate at less-than-optimal speed because of their energetic proximity to the bulk bands. Notably, as confirmed by long-range propagation simulations, this decreased density of states does not significantly increase the dispersive broadening of narrow excitations. Perhaps most surprisingly, the fractal speed enhancement persists even if the "edge" is supported only by a chain of first-generation Sierpinski gaskets (see figs. S10 and S11).

Having demonstrated the topologically protected edge states in a deterministic Sierpinski gasket, the question naturally arises as to whether there are any other fractal TI systems, and, if so, what unifying principles can be identified between them. Clearly, the degree of internal connectedness has to play a major role in this regard, because randomly removing large proportions of sites reliably destroys nontrivial characteristics of TI lattices as their bulk gradually disintegrates (*18*). Perhaps the most intriguing question is whether there is a critical value of the fractal dimension below which TI characteristics are categorically precluded. As a first step toward charting the varied landscape of fractal topology, we studied several other fractal systems with dimensions above as well as below the value $d = \log_2 3 \approx 1.58$. To that end, we numerically calculated their eigenmodes in the presence of a magnetic flux and simulated the dynamics of edge modes in the presence of disorder to verify their topological features (see fig. S12). We found that both the Sierpinski carpet ($d \approx 1.89$) and hexagon ($d \approx 1.63$) display chiral edge modes, whereas the triflake ($d \approx 1.26$) does not. We note that, in contrast to the gasket, topological transport of light in the carpet (see fig. S13) occurs in the anomalous Floquet TI regime (*23*). For the class of Sierpinski fractal systems, the gasket has the lowest dimension that allows for topological edge transport.

Similarly, these questions can also be pursued for random fractals, where topological edge states were recently reported (*30*) to exist

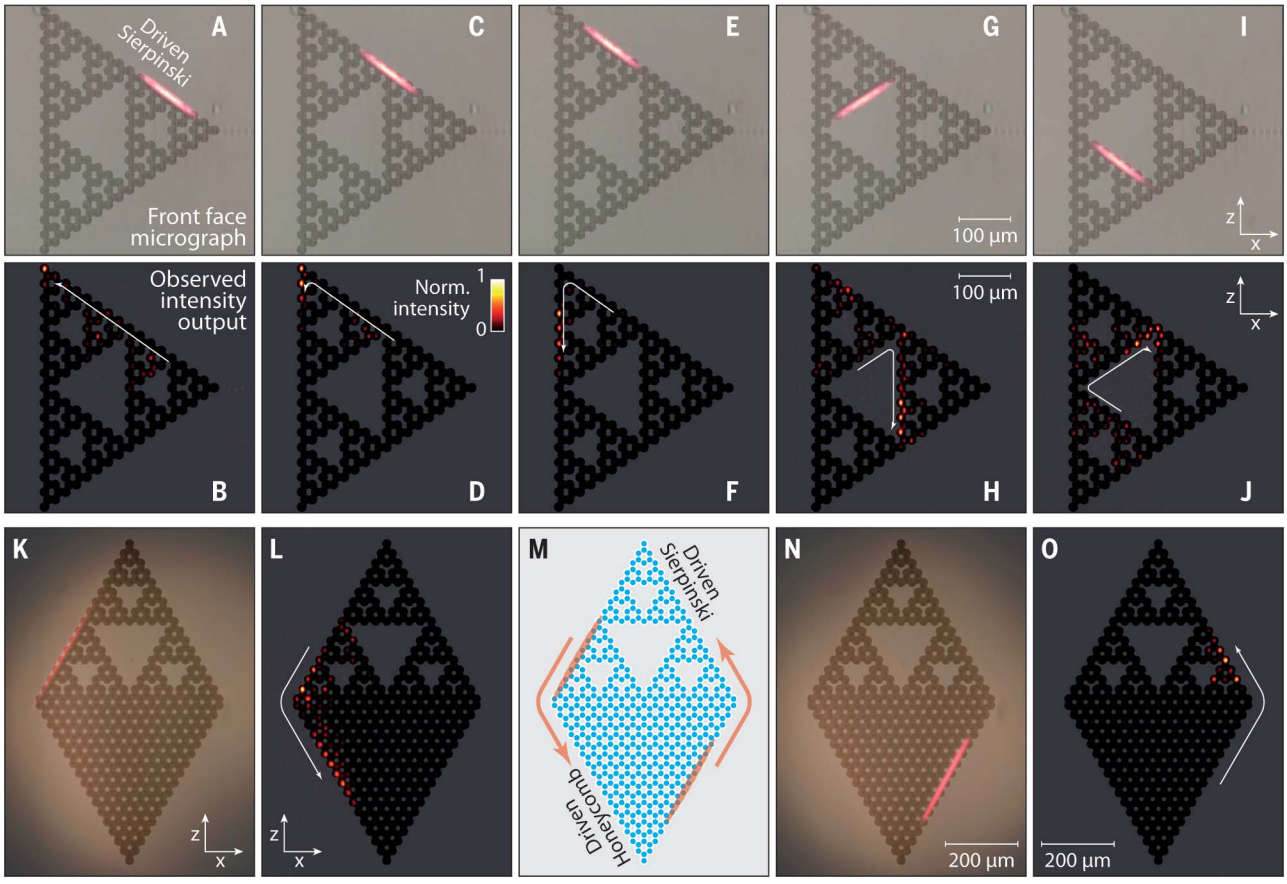

Fig. 3. Topological edge transport in the Sierpinski lattice. (**A** to **F**) By varying the position of a broad Gaussian excitation along the outer perimeter, we observe unidirectional counterclockwise propagation of the perimeter state around the upper corner. (**G** to **J**) Likewise, varying the excitation position at the central inner edge yields unidirectional transport with the opposite (clockwise) chirality (see fig. S4 for additional measurement data and a direct comparison to the honeycomb). (**K** to **O**) Transport in a hybrid fractal-honeycomb lattice. Placing a broad beam with an appropriately tilted phase front at the front facet of a rhombic lattice composed of a Sierpinski gasket in its upper half and a honeycomb lattice in its lower part allows for a direct excitation of the topological edge state. Light injected into the fractal domain passes the corner marking the border between the two lattices (K) and continues along the edge of the honeycomb with virtually no bulk leakage (L). Despite the fundamentally different lattice geometries in the two domains, the helically driven hybrid structure (M) supports a joint edge state along its outer perimeter. Similarly, an edge wave packet launched in the honeycomb domain (N) continues along the outer edge of the Sierpinski domain (O). The front-face micrographs show the placement of the excitation beam, whereas the output intensities were observed after propagation through the 150-mm-long sample. In all panels, the outline of the waveguide arrays is indicated by a semitransparent overlay as a guide to the eye.

in two-dimensional percolation clusters with $d \approx 1.90$. Our studies confirm that recent theoretical finding but do not indicate any other topological random fractal systems below this value. Given the above results, it seems that for deterministic (exact) fractals constructed from straight lines, the Sierpinski gasket marks the lower bound for topological behavior. Moreover, because the only known example of a topological random fractal features a Hausdorff dimension substantially closer to $d = 2$, $d = \log_2 3$ may be a more general threshold. Certainly, the role of the dimension for fractal TIs and its interplay with randomness merit further theoretical as well as experimental study.

We have reported on the observation of a fractal TI and showed that even structures that lack any conventional bulk can support topologically protected edge states when subjected to an appropriate Floquet drive. Our results highlight the fundamentally different nature of fractal TIs that radically departs from the established understanding that largely depends on the bulk-edge correspondence. The complete absence of a bulk not only fails to hamper the existence of topologically protected states along the outer perimeter but also actually enables a whole hierarchy of internal edges within. By breaking the link between increased edge conductance and suppressed bulk transport, the self-similar structure of the Sierpinski gasket serves to boost the mobility of the topological edge channel. The experiments presented here constitute only the first of many steps in the experimental exploration of topological phenomena in systems with noninteger dimensionality. We envision an entirely new generation of hybrid systems that fruitfully combine the robustness and protection of conventional TIs with new degrees of freedom arising from self-similarity. Beyond photonic applications, where fractal designs may accelerate protected transport and enable precisely tailored topological band structures for high-end sensing devices, similar ideas may inspire methods for the synthesis of advanced topological materials that harness self-organized processes, for example, in thin-film deposition (*26*) or cluster formation (*30*). The key questions to tackle in this regard will be under which circumstances a given fractal is a suitable host lattice for topological edge states and whether there is an underlying set of general rules that governs which types of fractals are fundamentally capable of topological behavior.

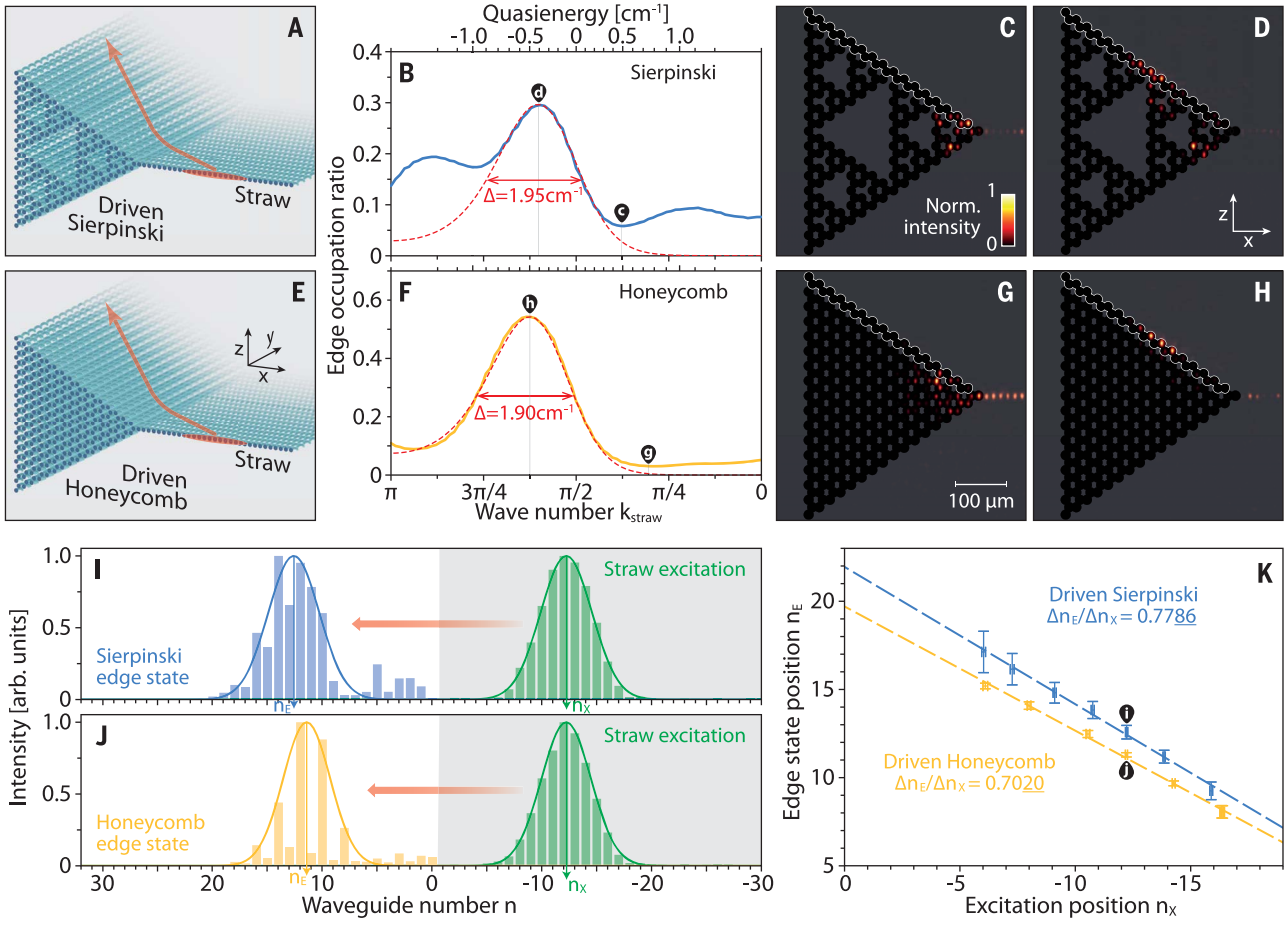

Fig. 4. Edge-state spectroscopy and velocity in topological fractals. (**A**) Broad-beam excitations in planar "straw" arrays appended to a corner of the driven Sierpinski gasket serve to synthesize wave packets with a narrow *k*-space spectrum, allowing for specific quasi-energies to be addressed by selecting an appropriate wavefront tilt (for details, see figs. S5 and S6). (**B**) Measured edge-state occupation ratio at the end of the 150-mm-long sample. (**C**) Quasi-energies outside the topological gap allow light to diffract deep into the lattice. (**D**) By contrast, excitations within the gap yield a pronounced population of the topological edge state near the resonant angle of excitation. A certain leakage into the lattice interior occurs because of the presence of internal topological edge states with similar quasi-energies. (**E** to **H**) Applying the same excitation conditions to the honeycomb shows that, whereas mismatched excitations primarily populate the bulk of the lattice (G), a substantial fraction of the injected light is deposited into the topological edge state (H). In (C), (D), (G), and (H), the lattice outlines, excluding the straws, are indicated by semitransparent overlays as a guide to the eye, and the sites that were evaluated for the edge occupation ratio are outlined in white. In (B) and (F), the width of the respective resonances was measured as full width at half maximum of a Gaussian fit in the quasi-energy (dashed red lines; see fig. S7 for the plot with a linear energy scale). (**I** and **J**) A direct comparison for equivalent excitation conditions shows that the Sierpinski edge state systematically outpaces its conventional counterpart. (**K**) A series of measurements with varying placement of the broad Gaussian excitation, indicated by its initial central position n_X within the straw, shows that the fractal topological edge transport is about 11% faster than it is in the honeycomb lattice. More details on these measurements are provided in figs. S8 and S9.

REFERENCES AND NOTES

1. M. Z. Hasan, C. L. Kane, *Rev. Mod. Phys.* **82**, 3045–3067 (2010).
2. Z. Wang, Y. Chong, J. D. Joannopoulos, M. Soljačić, *Nature* **461**, 772–775 (2009).
3. M. Hafezi, E. A. Demler, M. D. Lukin, J. M. Taylor, *Nat. Phys.* **7**, 907–912 (2011).
4. A. B. Khanikaev *et al.*, *Nat. Mater.* **12**, 233–239 (2013).
5. M. C. Rechtsman *et al.*, *Nature* **496**, 196–200 (2013).
6. G. Jotzu *et al.*, *Nature* **515**, 237–240 (2014).
7. R. Süsstrunk, S. D. Huber, *Science* **349**, 47–50 (2015).
8. Z. Yang *et al.*, *Phys. Rev. Lett.* **114**, 114301 (2015).
9. Y. Hadad, J. C. Soric, A. B. Khanikaev, A. Alù, *Nat. Electron.* **1**, 178–182 (2018).
10. S. Klembt *et al.*, *Nature* **562**, 552–556 (2018).
11. A. Bundle, S. Havlin, Eds., *Fractals in Science* (Springer, 1994).
12. M. V. Berry, *J. Phys. Math. Gen.* **12**, 781–797 (1979).
13. G. P. Karman, G. S. Mcdonald, G. H. C. New, J. P. Woerdman, *Nature* **402**, 138 (1999).
14. O. Mendoza-Yero *et al.*, *Opt. Lett.* **37**, 1145–1147 (2012).
15. X.-Y. Xu, X.-W. Wang, D.-Y. Chen, C. M. Smith, X.-M. Jin, *Nat. Photonics* **15**, 703–710 (2021).
16. Y. Xie *et al.*, *APL Photonics* **6**, 116104 (2021).
17. W. Sierpinski, *Compt. Rend. Acad. Sci. Paris.* **160**, 302–305 (1915).
18. Z. Yang, E. Lustig, Y. Lumer, M. Segev, *Light Sci. Appl.* **9**, 128 (2020).
19. D. Levine, P. J. Steinhardt, *Phys. Rev. Lett.* **53**, 2477–2480 (1984).
20. B. Freedman *et al.*, *Nature* **440**, 1166–1169 (2006).
21. Y. Hatsugai, *Phys. Rev. Lett.* **71**, 3697–3700 (1993).
22. E. Park, *Complex Topological K-Theory*, vol. 111 of *Cambridge Studies in Advanced Mathematics* (Cambridge Univ. Press, 2008).
23. M. S. Rudner, N. H. Lindner, E. Berg, M. Levin, *Phys. Rev. X* **3**, 031005 (2014).
24. M. Fremling, M. van Hooft, C. M. Smith, L. Fritz, *Phys. Rev. Res.* **2**, 013044 (2020).
25. A. A. Iliasov, M. I. Katsnelson, S. Yuan, *Phys. Rev. B* **101**, 045413 (2020).
26. C. Liu *et al.*, *Phys. Rev. Lett.* **126**, 176102 (2021).
27. N. P. Mitchell, L. M. Nash, D. Hexner, A. M. Turner, W. T. M. Irvine, *Nat. Phys.* **14**, 380–385 (2018).
28. Z. Darázs, A. Anishchenko, T. Kiss, A. Blumen, O. Mülken, *Phys. Rev. E Stat. Nonlin. Soft Matter Phys.* **90**, 032113 (2014).
29. G. Harari *et al.*, *Science* **359**, eaar4003 (2018).
30. N. M. Ivaki, I. Sahlberg, K. Pöyhönen, T. Ojanen, arXiv:2112.08824v1 [cond-mat.mes-hall] (2021).
31. T. Biesenthal *et al.*, RosDok (2022); https://doi.org/10.18453/rosdok_id00003634.

ACKNOWLEDGMENTS

We thank C. Otto for preparing the high-quality fused silica samples that were used for the inscription of all photonic structures used in this work. **Funding:** Deutsche Forschungsgemeinschaft grants SCHE 612/6-1 (A.S.), SZ 276/12-1 (A.S.), BL 574/13-1 (A.S.), SZ 276/15-1 (A.S.), SZ 276/20-1 (A.S.), and SFB 1477 "Light-matter interactions at interfaces," project number 441234705 (A.S. and M.H.); the Krupp von-Bohlen-and-Halbach Foundation

(A.S.); National Science Foundation of China grant 12174339 (Z.Y.); and Fundamental Research Funds for the Central Universities (Z.Y.). **Author contributions:** Conceptualization: M.S., A.S., Z.Y.; Formal analysis: T.B., M.H., Z.Y.; Investigation: T.B., M.H., L.J.M.; Visualization: M.H., T.B.; Funding acquisition: A.S., M.H., Z.Y.; Software: Z.Y., T.B.; Supervision: A.S., M.S.; Writing – original draft: T.B., L.J.M., Z.Y., M.K., M.S., A.S., M.H.; Writing – review and editing: M.H., A.S., M.S. **Competing interests:** The authors declare no competing interests. **Data and materials availability:** Experimental and simulation data not provided in the text or the supplementary materials can be found at the Rostock University Publication Server repository (*31*).

SUPPLEMENTARY MATERIALS

science.org/doi/10.1126/science.abm2842

Materials and Methods
Supplementary Text
Figs. S1 to S13
References (*32*–*55*)

Submitted 6 September 2021; resubmitted 7 February 2022
Accepted 3 May 2022
Published online 12 May 2022
10.1126/science.abm2842

Science

Fractal photonic topological insulators

Tobias BiesenthalLukas J. MaczewskyZhaoju YangMark KremerMordechai SegevAlexander SzameitMatthias Heinrich

Science, 376 (6597), • DOI: 10.1126/science.abm2842

Fractal topology

Topological insulators are formed with insulating bulk states surrounded by conducting surfaces. The insulating bulk states were thought to be crucial, stemming from the theoretical framework of the bulk-boundary correspondence; however, Biesenthal *et al*. found that need not be the case. Using a fractal structure in which there is no "bulk" as such, and thus no bulk insulating states, they show nonetheless that there are chiral conducting states confined to the edge. The results provide a possible new route to manipulate the topological transport of light with engineered structures. — ISO